2

STATUS REPORT

SR-5

Period: July 31, 1972 through January 31, 1973

A STUDY OF THE LOCAL PRESSURE FIELD IN TURBULENT SHEAR FLOW AND ITS RELATION TO AERODYNAMIC NOISE GENERATION

Research Grant No. NASA NGR 14-005-149

Nuclear Engineering Program
and
Mechanical Engineering Department
University of Illinois at Urbana-Champaign
Urbana, Illinois 61801

Prepared by: Barclay G. Jones, Professor
H. Peter Planchon, Jr., Graduate Research Assistant

Research Conducted by: B. G. Jones, H. P. Planchon, D. P. Weber, R. J. Hammersley, D. Satterwhite, and R. Krich

Submitted and Approved by: Barclay G. Jones
Barclay G. Jones
Principal Investigator

TABLE OF CONTENTS

1. SCOPE AND OBJECTIVES 1

2. SUMMARY OF CURRENT STATUS 1

3. RESEARCH RESULTS 2

3.1 Pressure Transducer Error Analysis 2

3.2 Measurement Outline 8

3.3 Preliminary 6 in. Diameter Jet Results 9

3.3.1 Nozzle Exit Conditions 10

3.3.2 Mean Velocity Field 10

3.3.3 Fluctuating Velocity Field 11

3.3.4 Fluctuating Static Pressure Field 12

3.3.5 Pressure Space Time Correlations 12

4. FUTURE RESEARCH 13

5. REFERENCES 14

6. FIGURES

1. SCOPE AND OBJECTIVES

Aerodynamic noise sources in free shear layers are being studied by experimentally examining the turbulent fluid fields which are responsible for the sound generation. Primary emphasis is being placed on expressing the sound source in terms of the turbulent fluctuating pressure correlation in the Ribner[1*] dilitational formulation. The specific flow regimes being studied are the plain and annular two-stream mixing layers which comprise the high noise source region found in the first few diameters of a simple round jet or the more complex circular bypass jet.

The experimental and analytical program is directed to three interrelated efforts. The first is to experimentally determine the pressure and some velocity space-time correlations in the two-stream mixing layer. The second is to model the pressure space-time correlations in a form suitable for use in and examination of the Ribner dilitational formulation of noise generation. The third is to examine the ability of the model to predict the intensity and both spatial and spectral distributions of far field sound under various flow configurations and conditions.

2. SUMMARY OF CURRENT STATUS

Work during the period of this report has been in three areas: (1) pressure transducer error analysis, (2) fluctuating velocity and pressure measurements in the NASA Lewis 6-inch diameter quiet jet facility, and (3) measurement analysis.

A theory has been developed and experimentally verified to quantify the pressure transducer velocity interference error. The theory and supporting experimental evidence show that the errors are a function of the velocity field's turbulent structure. It is shown that near the mixing layer center the errors are negligible.

Turbulent velocity and pressure measurements were made in the NASA Lewis quiet jet facility. Some preliminary results are included in this report. The velocity field results are mediocre but usable for comparison. The lack of precision in these results stems primarily from the less than favorable

---

*Literature citations are shown by raised numbers corresponding to entries in REFERENCES.

measuring conditions and our unfamiliarity with the outdoor facility. The turbulent pressure results, however, seem to be of excellent quality. The better quality is due primarily to the ruggedness and inherently stable sensitivity of the pressure transducer.

3. RESEARCH RESULTS

This section includes details of the research program relating to documentation of the error analysis of the Pressure Transducer which shows its adequacy for sound source measurements. In addition, the program of measurements made on the 6-inch diameter jet is presented and followed by preliminary data presentation of results from the experiment.

3.1 Pressure Transducer Error Analysis

Use of the much simpler dilatation source model has been hampered by the lack of a suitable turbulent flow field fluctuating pressure measuring device. The requirements for such an instrument are rather severe. It must measure pressure in, and present minimal disturbance to, a flow volume which is very small compared to the turbulent scales of interest. The frequency response of the instrument should be flat in the range of interest. Finally, the direct response to the fluctuating velocity field should be negligibly small. A miniature pressure transducer has been developed which appears to meet these requirements for turbulent free mixing layers.

The pressure transducer is shown in Fig. 1. The structural and design details are given by Spencer and Jones[2]. The transducer operates from bleeding air in laminar flow through a capillary tube from a constant pressure reservoir. Pressure fluctuations at the capillary down stream end set up fluctuating velocities in the bleed fluid which are measured by a hot film sensor mounted across the exit of the capillary tube. The pressure transducer is fitted with a static pressure tip to minimize response to velocity fluctuations. The bleed fluid flows through the tip and exits via six circumferential bleed holes.

The pressure transducer meets the requirements that its size must be much smaller than the turbulent space scales of interest. For example, Laurence[3] shows that within the mixing region of a round jet the transverse velocity space scale L_r is given by $L_r = 0.036x$. Here x is the axial distance

from the lip of the jet. At x = 24 in., L_r = 0.86 in. In comparison the diameter of the transducer is 0.06 in. and the length from the tip to bleed holes is 0.15 in. The well contoured, highly polished tip presents a minimum flow disturbance. The low bleed rate results in a very low volumetric injection rate of bleed fluid into the free stream (0.001 cubic inches/sec. per bleed hole). At very low free stream velocities (less than 50 fps) and high bleed rates (0.003 cubic inches/sec.) the effect of the bleed injection is seen as thickening of the probe boundary layer which results in a sensitivity to axial velocity fluctuations. However, at free stream velocities of interest (above 100 fps) and with lower bleed rates this effect is not discernible.

The frequency response of the pressure transducer is fixed by the size of the capillary tube and the hot film sensor. The inner diameter of the capillary was chosen using Uchida's[4] results for the response of a viscous fluid in tube flow to a time varying pressure gradient. The cavity volume and the diameter of bleed holes in the diffuser tip were sized to avoid acoustical resonance or filtering within the audio range.

The frequency response of the transducer was experimentally determined by comparing its response to a calibrated B & K 1/8 inch diameter microphone. The test was conducted within the intense (SPL = 130dB) uniform acoustic field produced by an audio speaker. The results of the test showed the response dropping off at about 3 dB/octave above 400 Hz. as shown in Fig. 2. Here Sp(f) is the sensitivity to pressure as a function of frequency. Sp(0) is the zero frequency sensitivity determined as the rate of change of D.C. output with respect to change in the bleed fluid reservoir back pressure. This sensitivity is constant throughout the operating range. A simple R-C high pass circuit with required cut-off frequency and slope was designed and constructed to flatten the frequency response from D.C. to 10 KHz. The improved response using this device is also shown in Fig. 2.

The relative phase lag of two pressure transducers and their RC filter circuits used for space-time correlations is important. For this reason, identical transducers and RC circuits were constructed. The flow resistance of the capillary tubes was determined prior to assembly to insure uniformity. Finally, with the transducers subjected to a sinusoidal acoustic field, the phase lag was shown to be less than 10 degrees over the frequency range of interest.

The largest problem in measuring fluctuating static pressure arises from the interaction of the fluctuating flow field with the surface of the instrument. Siddons[5] investigation indicates that this error for our pressure transducer can be modeled as a quasistatic, ideal flow, velocity-to-pressure conversion. The analytical and experimental results which follow show this is an applicable model, and that errors from this mechanism are small near the center of a mixing layer.

The essential assumptions of the model are:

a. The pressure transducer measures the pressures developed on its surface due to velocity-to-pressure conversion and static pressure in a linear combination.

b. The size of the surface area in question is small compared to the scale of velocity spatial variations.

c. The surface pressure due to velocity develops in a very short time and flow separation does not occur.

With these assumptions, the surface pressure distribution follows easily from a steady-state ideal flow analysis. Since the describing equation is linear, the effects of axial velocities and normal velocities can be separated and analyzed individually.

The functional relationship between axial velocity and pressure at the holes of a static pressure tube was developed by Prandtl. Dean[6] shows these results can be expressed as

$$P - P_\infty = A\ 1/2\rho U_A^2 \tag{1}$$

Here P is the pressure at the sensing holes, U_A^2 is the free stream axial velocity, and A is the pressure coefficient fixed by the accelerating influence of the hemispherical tip and the stagnating influence of the stem. Using figures in Dean[6] that quantify the stem and tip effects, the pressure sensing holes were located to produce $A \simeq 0$.

The pressure distribution caused by the cross component of velocity was approximated as the aximuthal pressure distribution on a long cylinder in ideal cross flow. The solution for the pressure distribution is

$$P - P_\infty = 1/2\rho V_N^2[1 - 4 \sin^2\phi] \tag{2}$$

Here V_N is the velocity component normal to the surface of the pressure transducer. The angle ϕ is measured from the center of the pressure transducer cross section between V_N and the other surface point in question. The effective pressure sensed is the average pressure of the six holes and can be shown to be

$$P - P_\infty = B\ 1/2\rho V_N^2\ ;\ B = -1.0 \tag{3}$$

It should be pointed out that for 3 or more holes the averaged result does not depend upon the relative orientation of ϕ and the holes. Combining Eq. 2 and 3 yields an expression for the pressure transducer response to the velocity field

$$E_p(t) = S_p[A\ 1/2\rho U_A^2(t) + B\ 1/2\rho V_N^2(t)] \tag{4}$$

$E_p(t)$ is the total voltage developed by the axial and normal fluctuating velocities. S_p is the sensitivity of the probe to pressure and is a negative number.

The applicability of the ideal flow model and the actual sizes of A and B were evaluated experimentally in smooth, steady flow. The coefficient A was evaluated by orienting the probe for a zero yaw angle and varying the axial velocity head $h_A = 1/2\rho U_A^2$. Fig. 3 shows the results of this test. We see the pressure transducer output response increasing at low velocities. This is thought to be a viscous nose effect. Near 100 fps, the response reaches an asymptotic value and the coefficient A is zero.

The pressure coefficient for transverse fluctuation was evaluated by varying the normal velocity component. This was accomplished by yawing the pressure transducer in a steady flow. For this case, Eq. 4 reduces to

$$E_p(\theta) - E_p(0) = S_p(B-A)1/2\rho U_A^2 \sin^2\theta \tag{5}$$

θ is the yaw angle and $E_p(0)$ is the voltage at zero yaw angle. The results of this test are shown in Fig. 4. This figure shows separation does not occur and that the form of Eq. 5 is valid for $\theta<16°$. For greater yaw angles, the separation phenomena was observed on an oxcilloscope as a distinctive, intermittant, low frequency phenomena. This phenomena has not been subsequently observed in turbulent flow measurements. The value of B varied from -1.1 to -0.85 for the different tests at mean velocities from 140 fps to 500 fps.

Good agreement with the theoretical value of B = -1.0 is observed. The variation in the experimental values is primarily from uncertainty in determining the yaw angle.

The objective of the velocity model in Eq. 4 is to predict the velocity induced error. It should be observed that this error is a function not only of the coefficients A and B, but also of the velocity structure of the turbulent field. The mean square error to mean square pressure ratio will be evaluated here for conditions at the center of a mixing layer.

Substituting mean and fluctuating components into Eq. 4 and substracting the mean component yields the fluctuating error

$$E_e(t) = E_p(t) - \overline{E_p(t)}$$

$$= \frac{S_p A\rho}{2}\left[2u_A(t)\,\overline{U}_A + u_A^2(t) - \overline{u_A^2(t)}\right]$$

$$+ \frac{S_p B\rho}{2}\left[2v_N(t)\,\overline{V}_N + v_N^2(t) - \overline{v_N^2(t)}\right] \qquad (6)$$

The long time average, denoted by an overbar, of the mean square of Eq. 6 is now obtained and the following turbulent structural constants are substituted

$$F_A = \frac{\overline{u_A^4}}{(\overline{u_A^2})^2} \quad ; \quad F_N = \frac{\overline{v_N^4}}{(\overline{v_N^2})^2} \quad ; \quad S = \frac{\overline{u_A^3}}{(\overline{u_A^2})^{3/2}}$$

$$I = \frac{(\overline{u_A^2})^{1/2}}{\overline{U}_A} \quad ; \quad K = \frac{\overline{v_N^2}}{\overline{u_A^2}} \quad ; \quad R_{v_N^2 u_A^2} = \frac{\overline{v_N^2 u_A^2}}{\overline{v_N^2}\;\overline{u_A^2}} \qquad (7)$$

$$f = \frac{(\overline{p^2})^{1/2}}{1/2\rho\overline{u_A^2}} = \frac{p'}{1/2\rho\overline{u_A^2}} \quad ; \quad R_{v_N^2 u} = \frac{\overline{v_N^2 u_a}}{K(\overline{u_A^2})^{3/2}}$$

The result is:

$$\overline{E_e^2} = S_p^2 \left\{ A^2\left(\frac{\rho}{2}\right)^2 \overline{(u_A^2)}^2 \left[\frac{4}{I^2} + \frac{4S}{I} + F_A - 1\right] + \right.$$

$$+ AB\left(\frac{\rho}{2}\right)^2 \overline{(u_A^2)}^2 \left[K \left(\frac{2\,R_{v_N^2 u_A}}{I} + R_{v_N^2 u_A^2} - 1\right)\right] + \qquad (8)$$

$$\left. + B^2\left(\frac{\rho}{2}\right)^2 \overline{(u_A^2)}^2 \left[(F_N - 1)\, K^2\right] \right\}$$

where it is assumed that $\overline{V_N} = 0$ by aligning the probes axis with the mean flow.

Assuming weak statistical connection between the velocity error and true static pressure, their ratio can be found.

$$\frac{\overline{E_e^2}}{\overline{E_p^2}} = \frac{1}{f^2} \left\{ A^2\left(\frac{4}{I^2} + \frac{4S}{I} + F_A - 1\right) + \right.$$

$$+ ABK \left(\frac{2\,R_{v_N^2 u_A}}{I} + R_{v_N^2 u_A^2} - 1\right) + \qquad (9)$$

$$\left. + B^2K^2 \,(F_N - 1) \right\}$$

Equation 26 was evaluated using Spencer's[7] (1970) data for the center of a self similar plane mixing layer. The results are

$$\frac{\overline{E_e^2}}{\overline{E_p^2}} = \frac{1}{f^2}\left[179\, A^2 + 1.125\, B^2\right] \qquad (10)$$

or if A = 0 and B = -1.0

$$\frac{\overline{E_e^2}}{\overline{E_p^2}} = \frac{1.125}{f^2} \qquad (11)$$

From our measurements in Figs. 10 and 13, f = 6 approximately. This results in a first order error approximation of

$$\frac{\overline{E_e^2}}{\overline{E_p^2}} \simeq .03 \qquad (12)$$

3.2 Measurement Outline

The objective of the measurements at NASA Lewis was to determine the velocity and pressure fields of the jet shear layer and to record the pressure and velocity space time correlation data necessary to model the shear layer. Far field acoustical data was planned by NASA Lewis staff for comparisons. Although inclement weather prevented taking the full set of data anticipated, the one point turbulent and mean velocity field of the jet was determined and the majority of the important pressure field measurements were completed.

The measurements were taken in a cartestan coordinate system shown in Fig. 5. Most of the measurements were made in the x-r plane in the lower shear layer. However, to verify symmetry and jet alignment, some impact tube mean velocity data was taken in the upper shear layer, as well as for "θ traverses".

As shown by the Fig. 5 single point mean and axial fluctuating velocities and fluctuating static pressure were measured throughout the x-r plane in the lower 1/2 of the jet. Selected points including the center of mixing (r=R) were recorded and analyzed on the NOVATRONICS spectral analyzer.

Two groups of pressure space-time data were recorded. The stationary pressure transducer for these groups was at x = 6 in. and x = 24 in., respectively. For several radial positions of the stationary transducer the other sensor was positioned in a sequence of axial, radial, and azimuthal separations.

Several difficulties were encountered with the hotwires and electronics during the experiment. Most of the difficulties were rather obvious, (e.g. flow entrained snowflakes usually break hotwires). Some were more subtle and, even though in some cases the cause or remedy is not fully understood, in the interest of current research activities at NASA Lewis the problems are described below.

A sensitivity drift in hotwire anemometry and an excessive breakage rate were evident. These difficulties were probably due to contamination of the large air supply. The drift occured over periods when little ambient temperature change occured that could have caused the electronics to drift. Breakage frequently occured at times when entrainment of outside particles, probe vibration, and anemometer instability could be eliminated as a cause. The pressure transducer did not experience problems of this type because its sensor is not exposed directly to the jet flow. However, during pressure measurements

a slow buildup of dirt film on the PT outside surface was observed. This buildup did not affect its operation but such a buildup would alter a hot-wire's sensitivity and, if the particles were large enough, break the wire.

A high frequency noise (hundreds of KHz) with low frequency repetition rate (in the hundreds of Hz range) was eliminated by discontinuing use of the Walkie-Talkie near the anemometry. Addition of preamplifiers prior to the long transmission to the data center also helped reduce electronic noise.

Anemometer electronic stability was also a problem. On cold days ($T < 20°F$) with the 0.00015 mil tungsten sensors it was found that the anemometers could not be adjusted for stability. An external checkout demonstrated that the anemometry system performed well in a heated building at 65°F. Since low temperatures following high moisture weather was well correlated, it was thought that condensation within the equipment or cabling was likely the cause. However, this seems unlikely because no problem was observed with hot film sensors such as used in pressure transducers and a 'meggering' of the cables showed that they were not moisture contaminated.

Temperature sensitivity was also evident in other electronic equipment. The Wesson DC voltmeter reading was found to differ 5% on overlapping scales. This difference occured only on cold days. The linearizer and true RMS meter took about 3 hours to stabilize when moved to the outside rig. It was found that the flow entrainment cooling of the equipment was significant, hence, the last hour of warmup and final adjustments were made with the jet at operating flow conditions.

As indicated earlier in this section, the purpose of including a description of these experimental difficulties is primarily to indicate the various problem areas precipitated by conducting detailed flow studies with anemometer instrumentation in open air facilities under adverse temperature and ambient conditions. These are in striking contrast to similar studies conducted in the laboratory.

3.3 Preliminary 6 in. Diameter Jet Results

Only a small fraction of the data has been analyzed. The data so far analyzed includes that describing the nozzle exit velocity profile and background turbulence, the point mean and fluctuating velocities, maps of the point fluctuating pressure, and a pressure space-time correlation.

3.3.1 Nozzle Exit Conditions

The nozzle exit conditions of immediate interest are the shape of the exit mean velocity profile, background turbulence intensity, and the nature of the nozzle exit boundary layer. These conditions were measured with a boundary layer hotwire probe 0.03 in. downstream of the jet exit plane.

The mean velocity profile shown in Fig. 6 is, for practical purposes, flat. The small rise which commences about an inch from the wall and maximizes at the boundary layer edge is probably caused by the boundary layer effectively changing the shape of the nozzle. Although additional data points would be desirable, Fig. 6 shows that the boundary layer thickness is bounded by 0.05 in. $< \delta <$ 0.025 in. A crude calculation demonstrates the interesting fact that the boundary layer momentum defect is compensated by the momentum increase outside the boundary layer so that $U_{\ell} \pi R^2 \simeq \int_0^R 2\pi r \bar{U}(r) dr$.

The background turbulence and the jet lip turbulence is shown in Fig. 7. The centerline value of turbulence intensity $\sim$ 0.01 was not corrected for electronic noise and hence should be considered an upper limit. The turbulence intensity is observed to sharply peak near the lip. The peak intensity of 0.05 is much lower than the intensity of 0.15 observed in the developed mixing layer further downstream. Oscilloscope traces indicate that the disturbance near the lip is not turbulent but is heavily sinusoidal and therefore transitional. The dominant frequency at the lip edge (r = 3.0 in.) was near 14 kHz.

3.3.2 Mean Velocity Field

The mean velocity field was mapped both with a small impact tube (0.06 in. dia. tip) and a single hotwire sensor. Each of these instruments has advantages, however, both can be in error. Hence the two sets of readings serve as mutual checks. The shape of the mean velocity profiles compare well as shown in Fig. 8. However, a radial position uncertainty of up to $\frac{r-R}{x} = 0.01$ is evident. This uncertainty was due to inadvertant shifts in the traversing mechanism between the days in which impact tube and hotwire measurements were taken. The shifts were discovered after the velocity data was taken. A careful daily alignment eliminated the problem for the subsequent pressure data.

The mean velocity was found to be roughly similar for axial distances greater than 6 in. This is shown in Fig. 9. The spread parameter

$\sigma = \sqrt{\pi} \frac{\partial(U/U_j)_{max}}{\partial(\frac{r-R}{x})}$ was found to be $\sigma = 11$ for hotwire data and $\sigma = 11.25$ for impact tube data. These values agree well with Liepman and Laufers' generally accepted value of $\sigma = 11.0$. The scatter in Fig. 9 is due to a combination of errors from hotwire sensitivity drift, instrument temperature drift, and probe positioning uncertainties. Based upon the agreement of σ and the scatter evident in Fig. 9 the mean velocities are believed to be accurate within about 5%.

3.3.3 Fluctuating Velocity Field

The fluctuating velocities were measured with a single hotwire. The results in Fig. 10 show that the axial fluctuating velocity approaches similarity for $x > 6$ in. Laurence's[3] data, for a Mach number of 0.4, compares favorably in both magnitude and shape of distribution. The radial shift between our and Laurence's results is partially due to a Mach number effect. Laurence's data indicates an increasing outward deflection of the mixing layer with increasing Mach number. The shift may also be partially due to the previously indicated positioning uncertainty.

The spectra of the velocity fluctuations were most satisfying. Figure 11 shows several spectra near the center of the mixing layer ($r = 3.0$ in.). It should be mentioned that the spectral function $F(f)\Delta f$ is defined as the fraction of the turbulent energy between $f - \frac{\Delta f}{2}$ and $f + \frac{\Delta f}{2}$. The spectra were generated from the output of the NASA Lewis 1/3 octave bandpass NOVATRONICS unit. The scaling of the spectra indicates a certain similarity of the turbulent structure and the lack of significant periodic noise. The -5/3 slope, indicative of the inertial subrange, is a well established turbulence phenomena and lends support to the accuracy of the spectra measurements.

The spectra at different radial positions across the mixing layer are shown in Fig. 11. The velocity used in this figure is twice the local mean velocity. The factor 2 allows comparison of Fig. 10 with Fig. 11. For points well within the mixing layer turbulence (i.e. $r = 1.5$ in., 3.0 in., and 4.0 in.) good scaling between the spectra is again observed. This is consistent with the concept that the turbulent space scales vary slowly with position in the heavy shear region. The jet centerline spectrum ($r = 0$) is quite different from those within the heavy shear region. The spectral peak near the edge of the mixing layer is similar to that observed by Jones, Hammersley, Planchon and Spencer[8] and may be explained as the convection of a large scale eddy structure.

3.3.4 Fluctuating Static Pressure Field

The map of the fluctuating static pressure field is shown in Fig. 12 and Fig. 13. These results indicate that pressure when normalized by the jet total driving head ($1/2\ \rho U_j^2$) roughly approaches similarity. The peaks of the pressure distributions occur very near the radius of the jet lip ($\frac{r-R}{x} = 0.0$). These peak intensities, as shown in Fig. 14, maximize near the jet lip then drop off rapidly in the first two diameters downstream. An asymptotic region is then observed which lasts for the remainder of the driven region to about 30 in. (or five diameters) downstream.

The pressure power spectral density was obtained in the same manner as was the velocity spectrum. The results for three axial positions near the mixing centerline are shown in Fig. 15. Although the spectral shapes are similar, a scaling like that for the velocity case $\left(\frac{F(f)U_j}{x} \text{ vs } \frac{fx}{U_j}\right)$ has been examined and found to be only marginally adequate. This point requires further investigation. The shape of the spectral curves is similar also to the velocity spectra near the jet centerline at the end of the potential cone (compare Fig. 11 for x = 30 in., r = 0 and Fig. 15 for x = 30 in., r = 3.0 in.). The peak frequency of the pressure spectrum ($f_{pk} \simeq 105$ Hz) is, however, lower than that for velocity ($f_{pk} \sim 315$ Hz).

3.3.5 Pressure Space Time Correlations

The pressure space time correlations provide the kernel for the Ribner theory prediction of far field sound. A description and understanding of these correlations is consequently very important.

A pressure space-time correlation $Rpp(\Delta x,\tau)$ near the center of the mixing layer is shown in Fig. 16. These results were obtained by fixing one pressure transducer at x = 24 in., r = 3.0 in. and separating the other probe axially. The axial distance between the probes is Δx. An aximuthal offset of 0.15 in. was used to minimize probe interference at small separations. The failure of the zero axial separation curve to approach 1.0 is probably due to the azimuthal offset although probe interference at small separations may contribute. The dotted envelope is the autocorrelation in the convected frame.

The pressure space correlation indicates the size and distribution of correlated pressure regions. It is defined as $R_{pp}(\Delta x,\tau=o)$ and is shown in Fig. 17. A space scale defined as the area under this curve to its first zero

crossing is L_{px} = 1.1 in. In comparison Laurence[3] found the transverse velocity scale at x = 24 in. to be L_{Uy} = 0.86 in.

Convection velocities of the fluctuating pressure are also defined by the space time correlation. For each axial separation the delay time of the convected frame envelope is plotted as in Fig. 18. The slope of this plot is interpreted as the convection velocity. As shown in Fig. 18, the convection velocity is constant for all axial separations. It is observed that the convection velocity slightly exceeds the local mean velocity (U_c/U_j = 0.635 while $\overline{U}/U_j$ = 0.58).

Further analysis of the 6 in. dia. jet data will be reported later and will be used to compare with information from smaller jets for examination of geometric scaling parameters.

4. FUTURE RESEARCH

Our future research follows directly from our previously stated objectives. Presently the large amount of pressure data gathered in the NASA LEWIS experiment is being analyzed. Concurrently some additional measurements in our local 2-1/2 in. dia. jet facility are being taken. These measurements in a well controlled indoors facility will hopefully provide more precise and detailed velocity data for comparisons with the associated static pressure field data.

After the measurements are completed and analyzed the pressure space-time correlations will be modeled for input into the source term in the Ribner theory.

5. REFERENCES

1. Ribner, H. S., "The Generation of Sound by Turbulent Jets," Advances in Applied Mechanics, H. L. Dryden, Ed., 8, (1964).

2. Spencer, B. W., and Jones, B. G., "A Bleed-Type Pressure Transducer for In-Stream Measurements of Static Pressure Fluctuations," Review of Scientific Instruments, 42, No. 4 (1971).

3. Laurence, J. C., "Intensity, Scale and Spectra of Turbulence in the Mixing Region of a Free Subsonic Jet," NACA TR-1292 (1956).

4. Ychida, S., "The Pulsating Viscous Flow Superimposed on the Steady Laminar Motion of Incompressible Fluid in a Circular Pipe," AZMP 8, (1956).

5. Siddon, T. E., "On the Response of Pressure Measuring Instrumentation in Unsteady Flow (An investigation of errors induced by probe flow interaction)," UTIAS Report 136 (1969).

6. Dean, R. C., Aerodynamic Measurements, M.I.T. Press, Cambridge, Mass. (1953).

7. Spencer, B. W., "Statistical Investigation of Turbulent Velocity and Pressure Fields in a Two-Stream Mixing Layer," Ph.D. Thesis, University of Illinois at Urbana-Champaign, (1970).

8. Jones, B. G., Hammersley, R. J., Planchon, H. P., and Spencer, B. W., "The Turbulence Structure in the Plane Two-Stream Mixing Layer," Proceedings of the ASME Symposium on the Fluid Mechanics of Mixing, Atlanta, Ga., June 20-22 (1973).

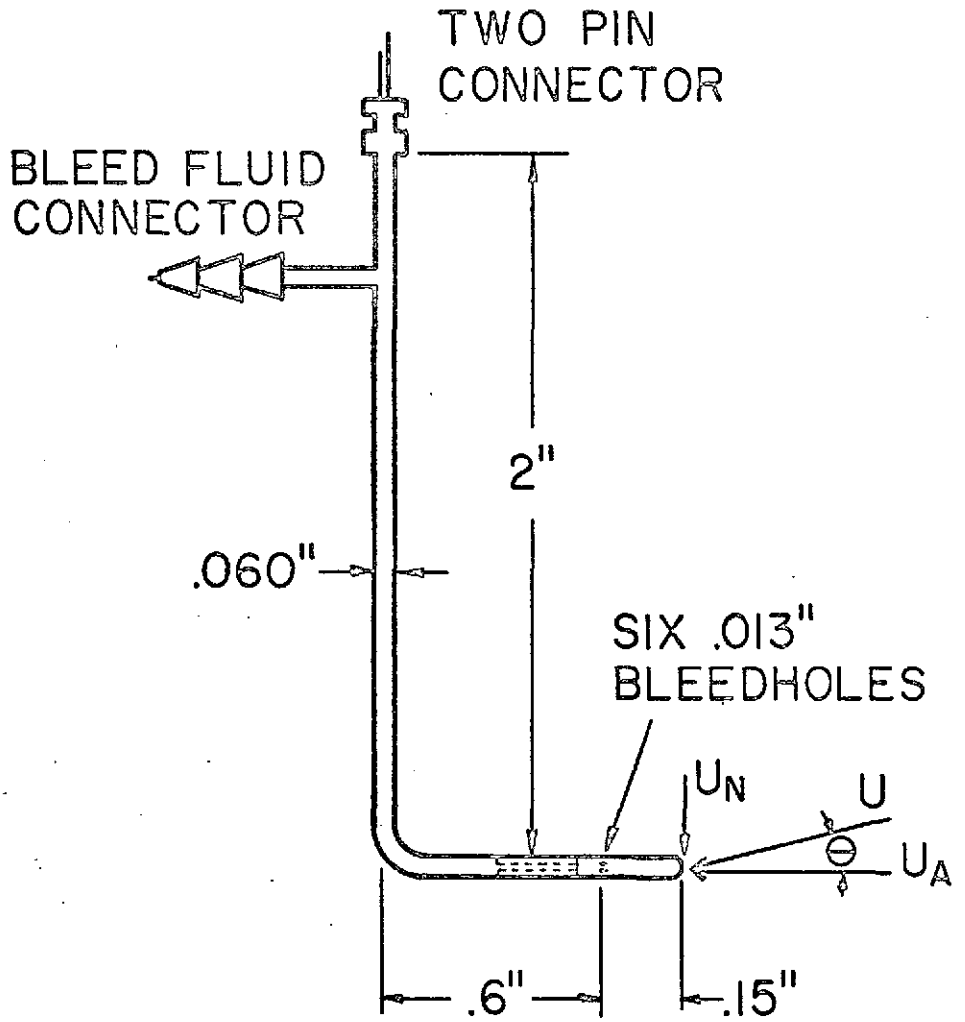

Fig. 1 Schematic of pressure transducer (PT)

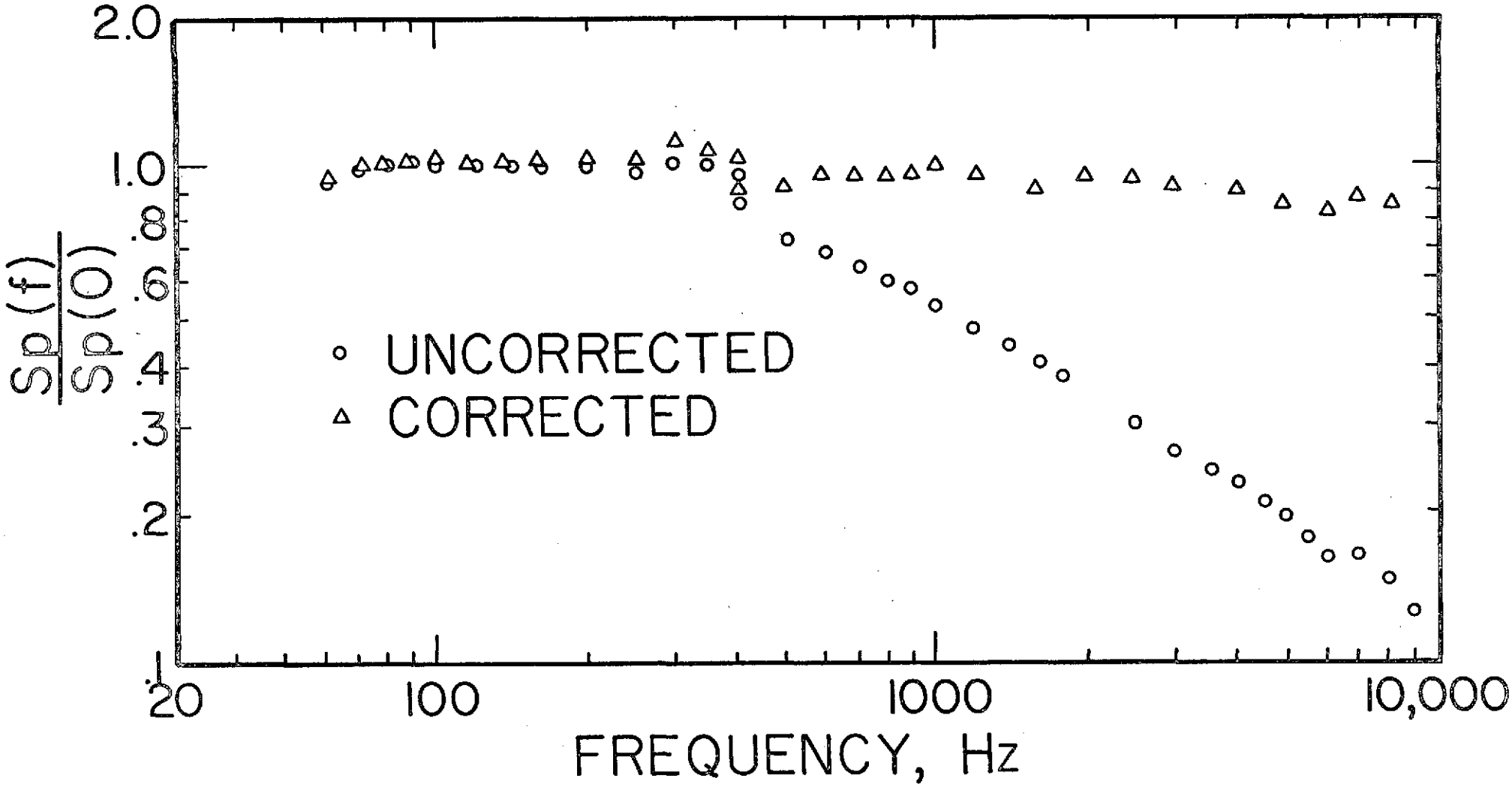

Fig. 2 Pressure transducer frequency response

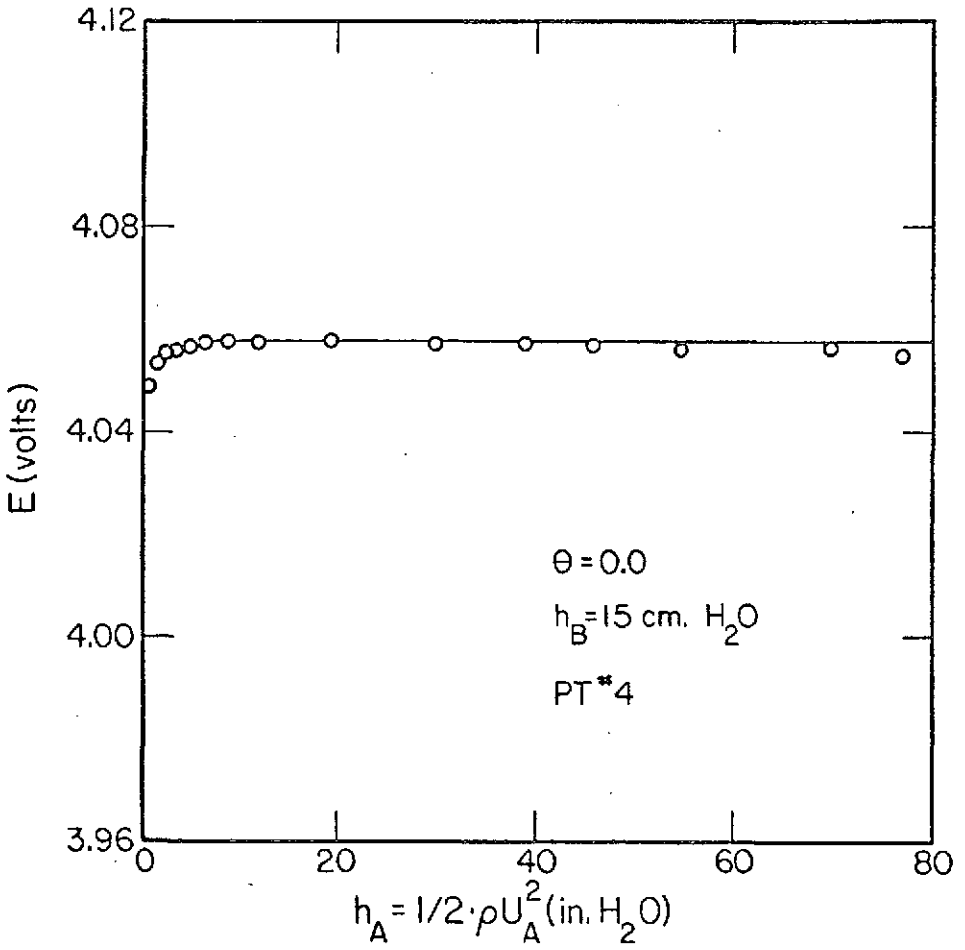

Fig. 3 Pressure transducer response to axial velocity

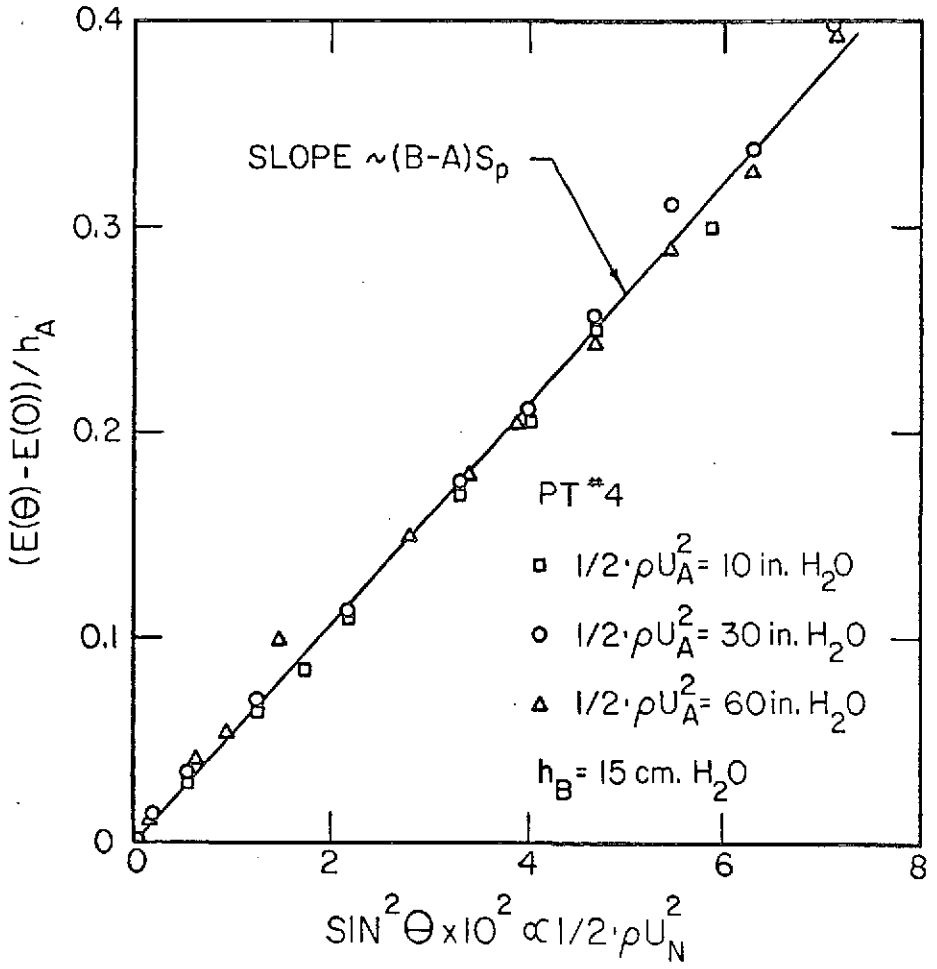

Fig. 4 Pressure transducer response to transverse velocity

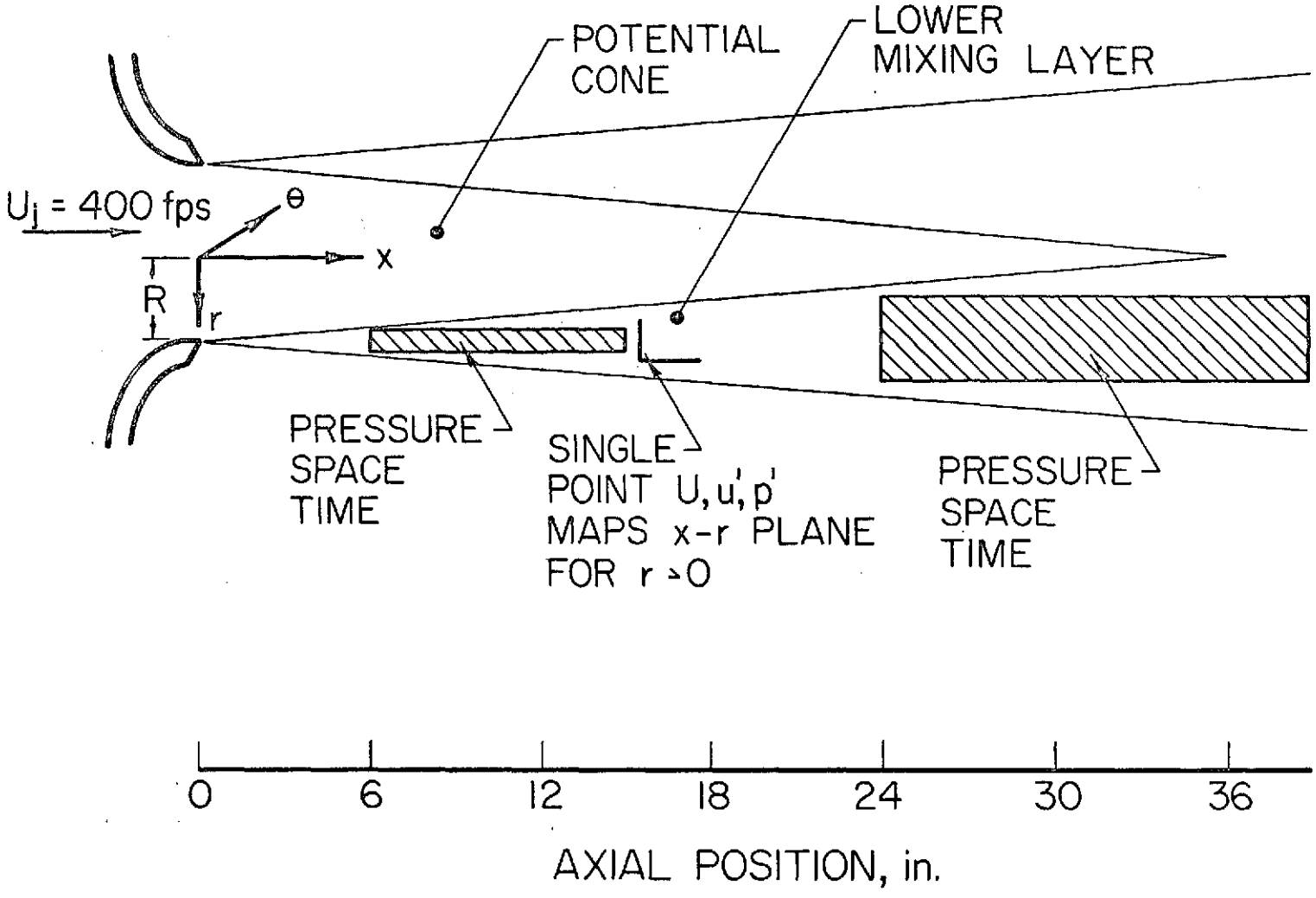

Fig. 5 Jet geometry and measurement positions.

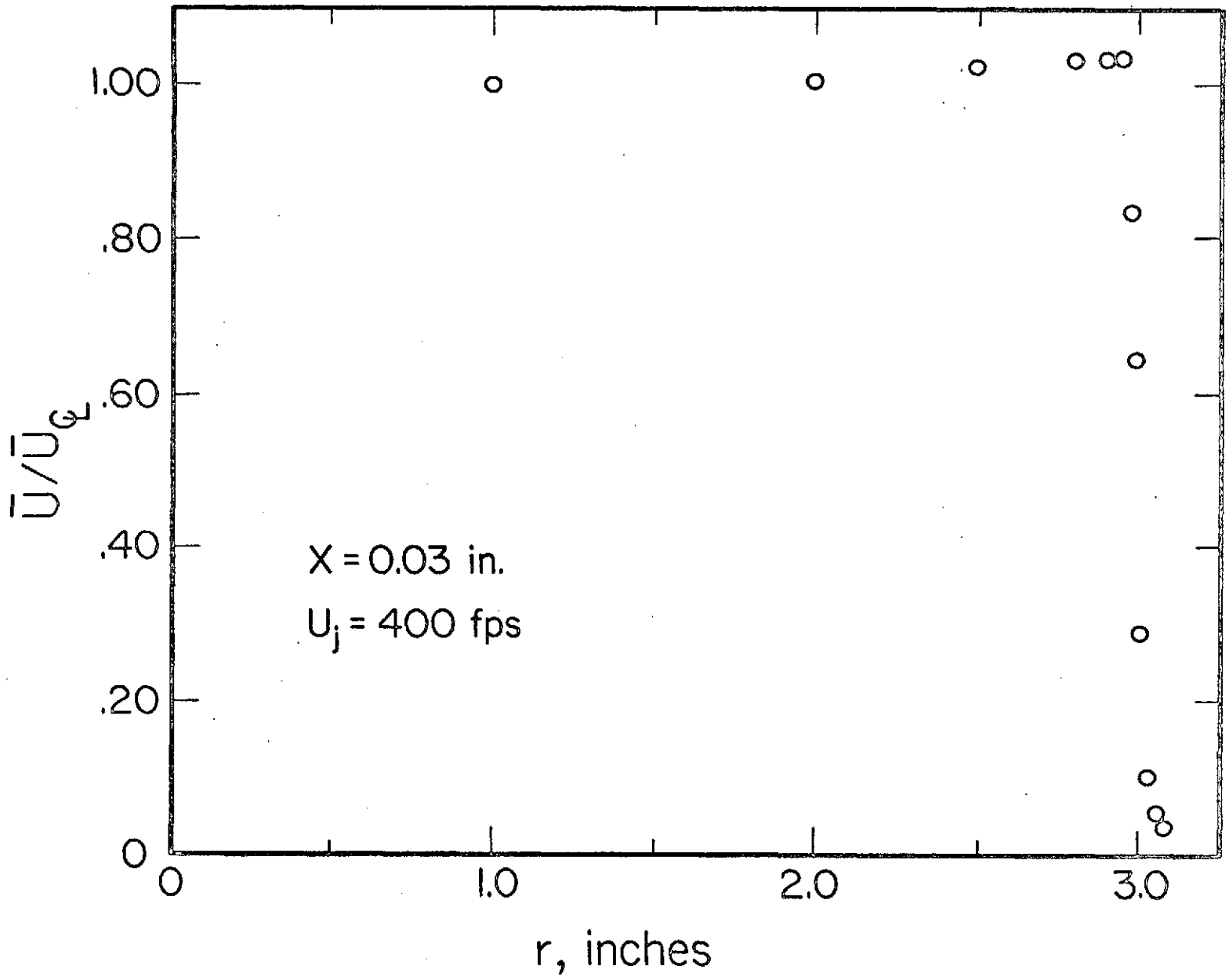

Fig. 6 Exit plane velocity profile (NASA 6 in. dia. jet)

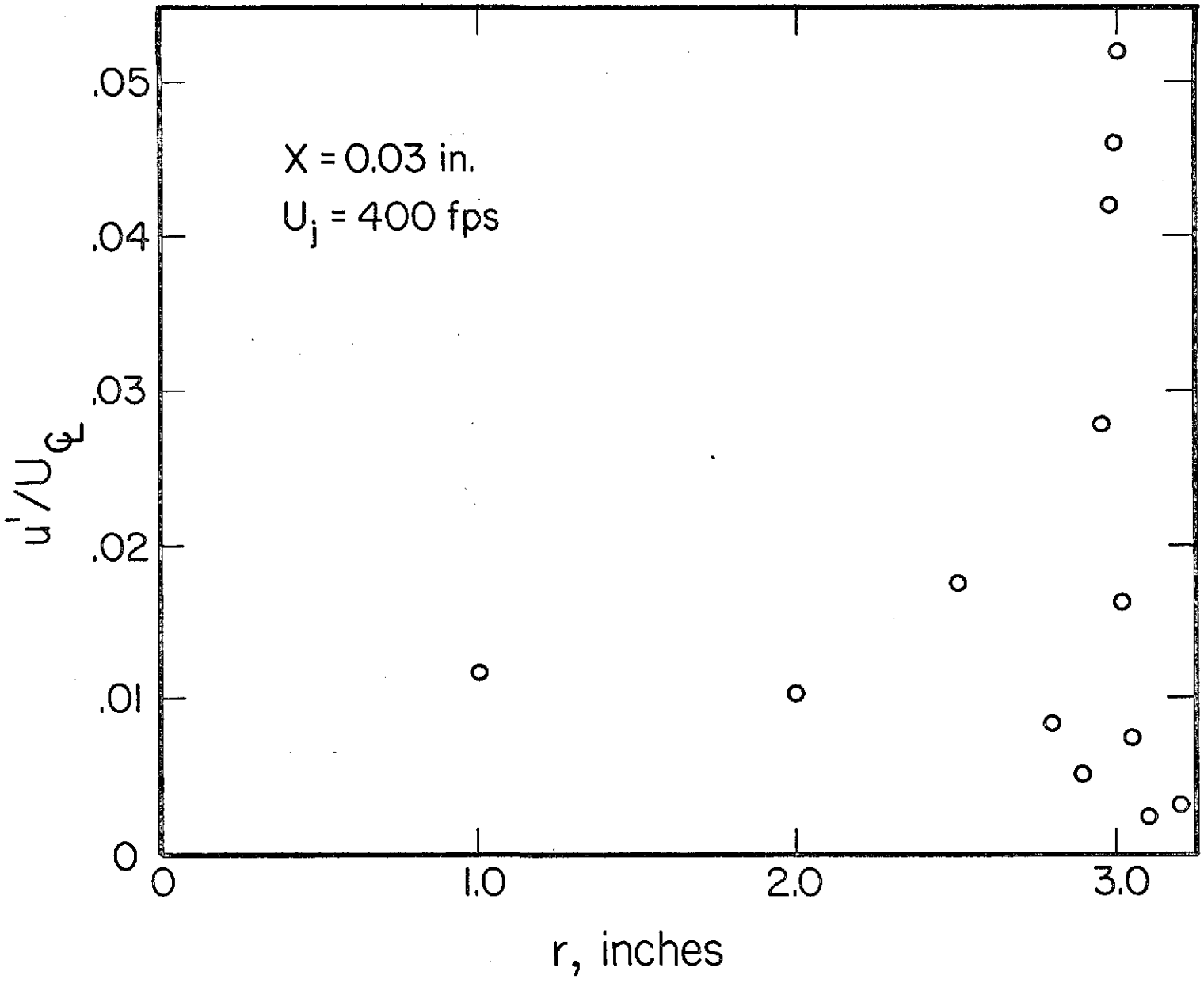

Fig. 7 Exit plane axial velocity turbulence intensity (NASA 6 in. dia. jet)

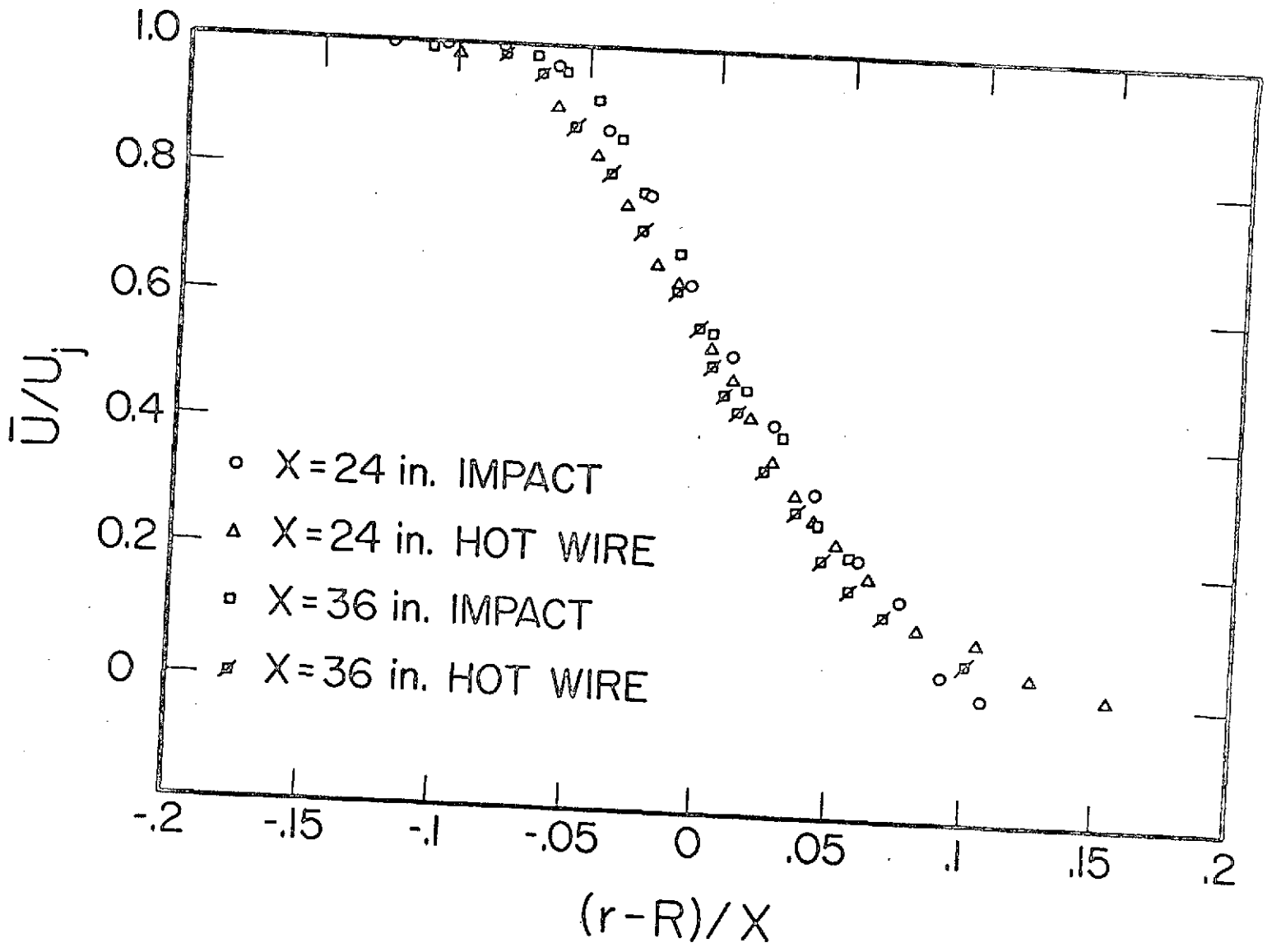

Fig. 8 Impact tube and hot wire mean velocity comparison (NASA 6 in. dia. jet, R = 3 in.)

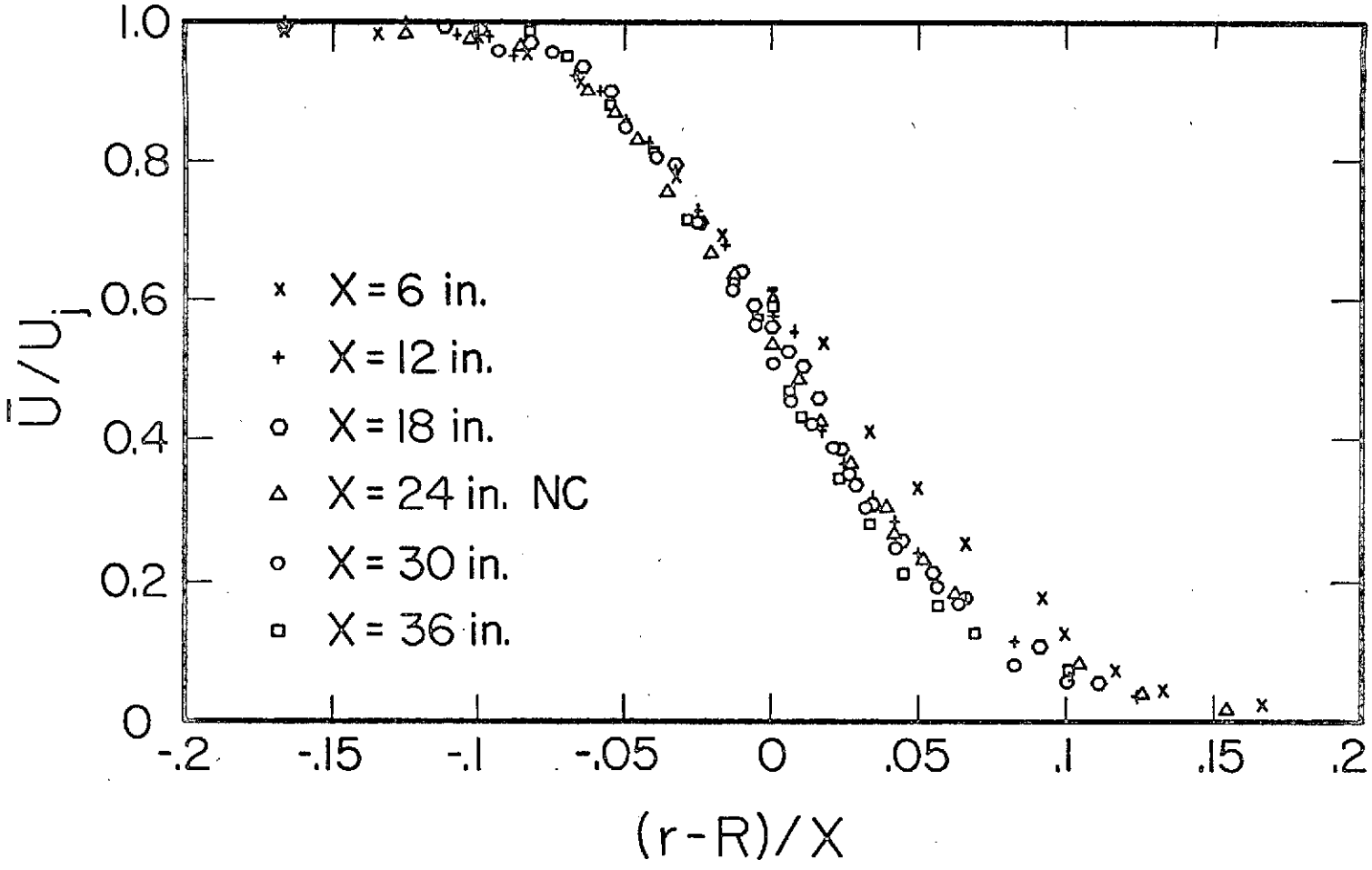

Fig. 9 Mean velocity profiles (NASA 6 in. dia. jet: $U_j \approx 400$ fps, R = 3 in.)

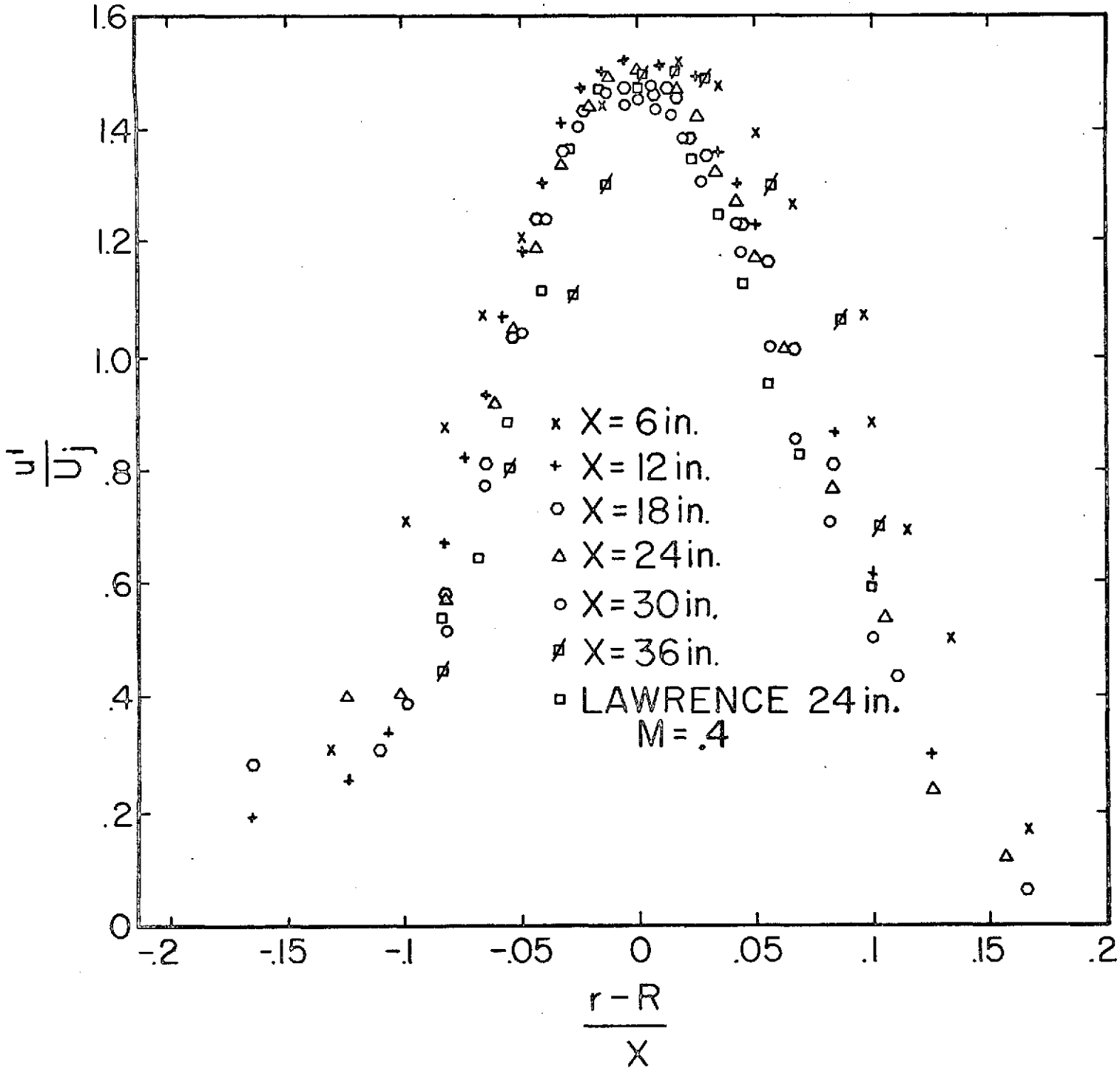

Fig. 10 Axial velocity turbulence intensity profiles (NASA 6 in. dia. jet: $U_j \simeq 400$ fps, R = 3 in.)

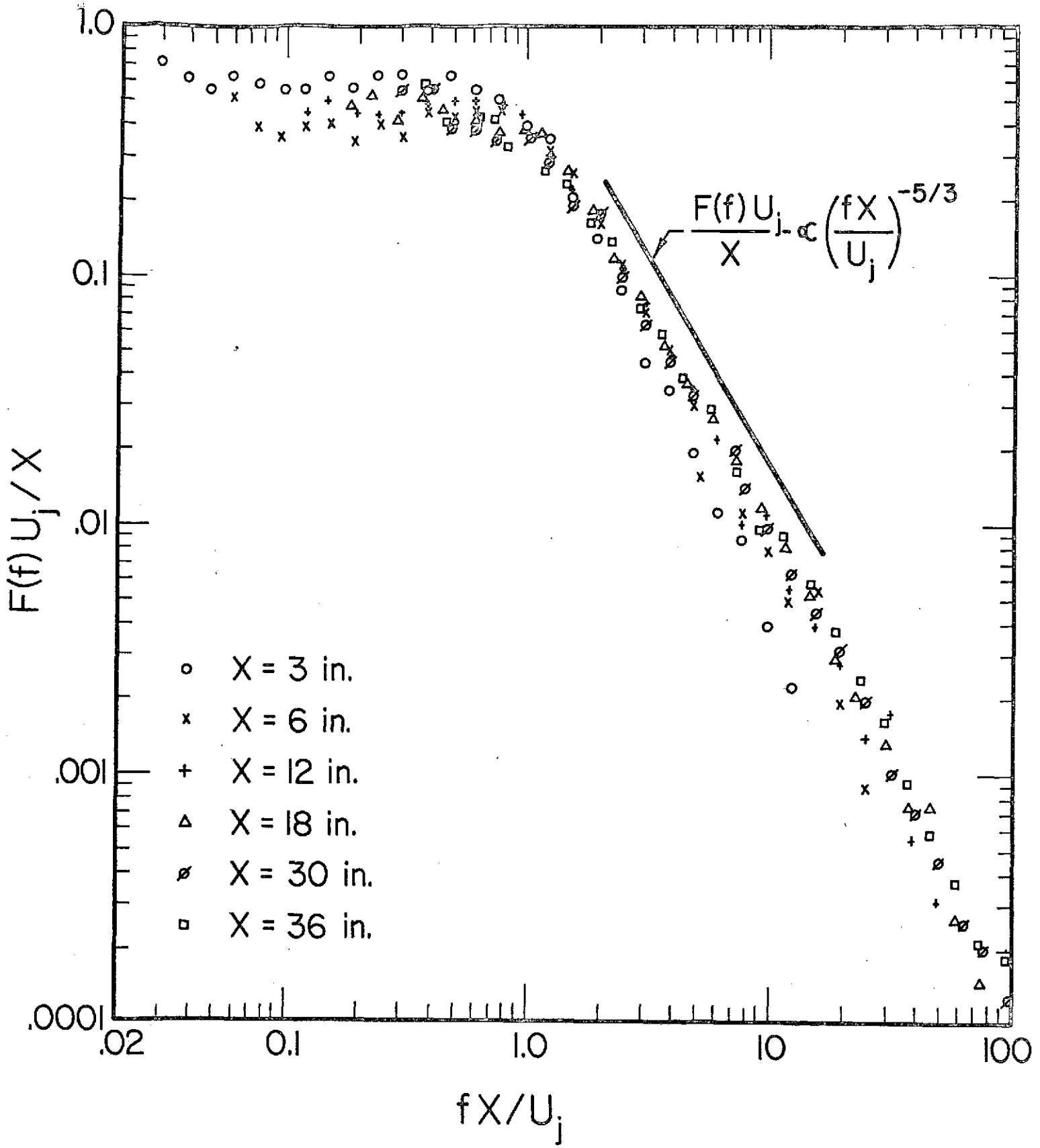

Fig. 11 Axial velocity turbulence spectra at mixing centerline (NASA 6 in. dia. jet: U_j = 400 fps, r = 3.0 in.)

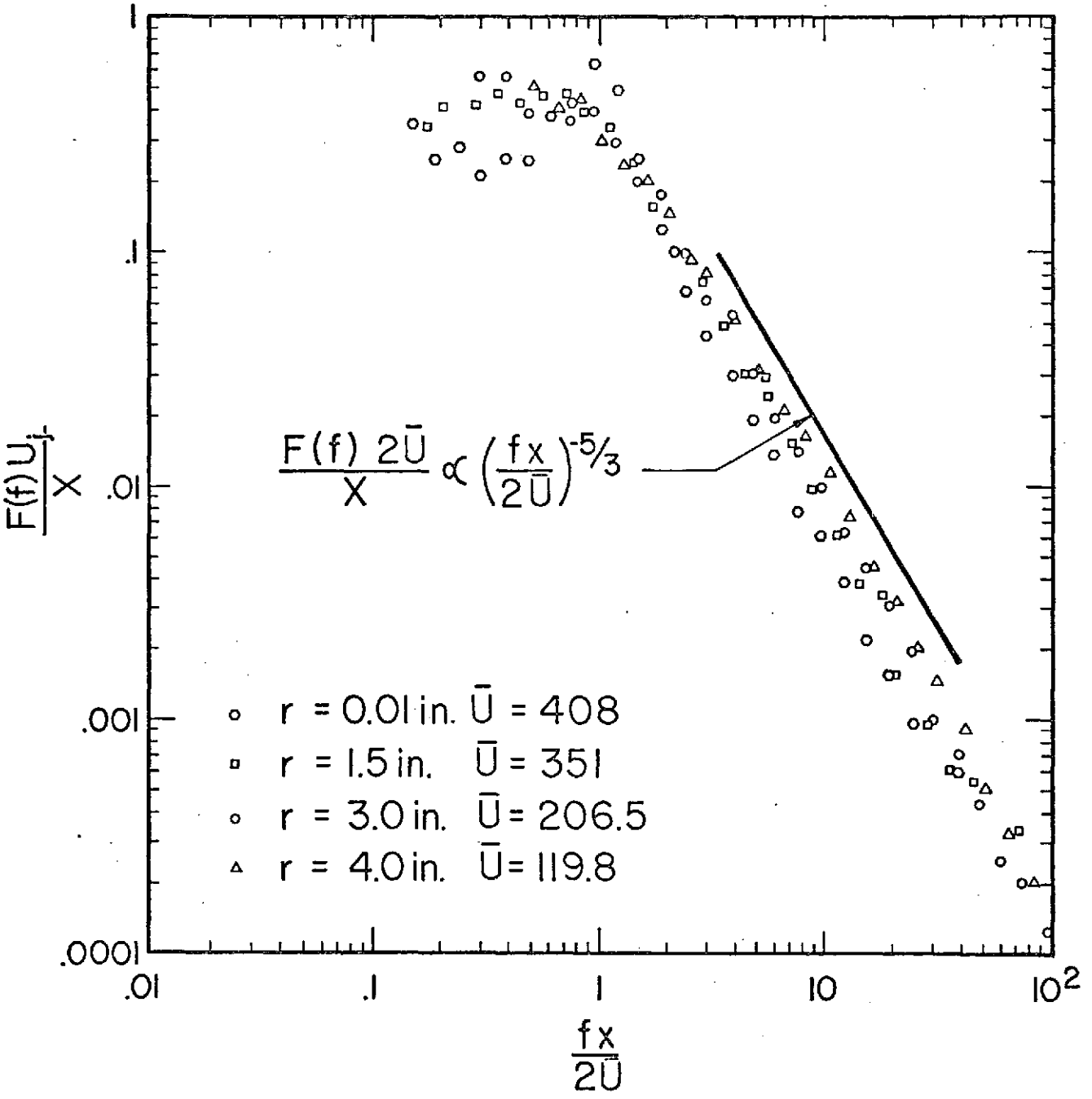

Fig. 12 Axial velocity turbulence spectra (NASA 6 in. dia. jet: X = 30 in.)

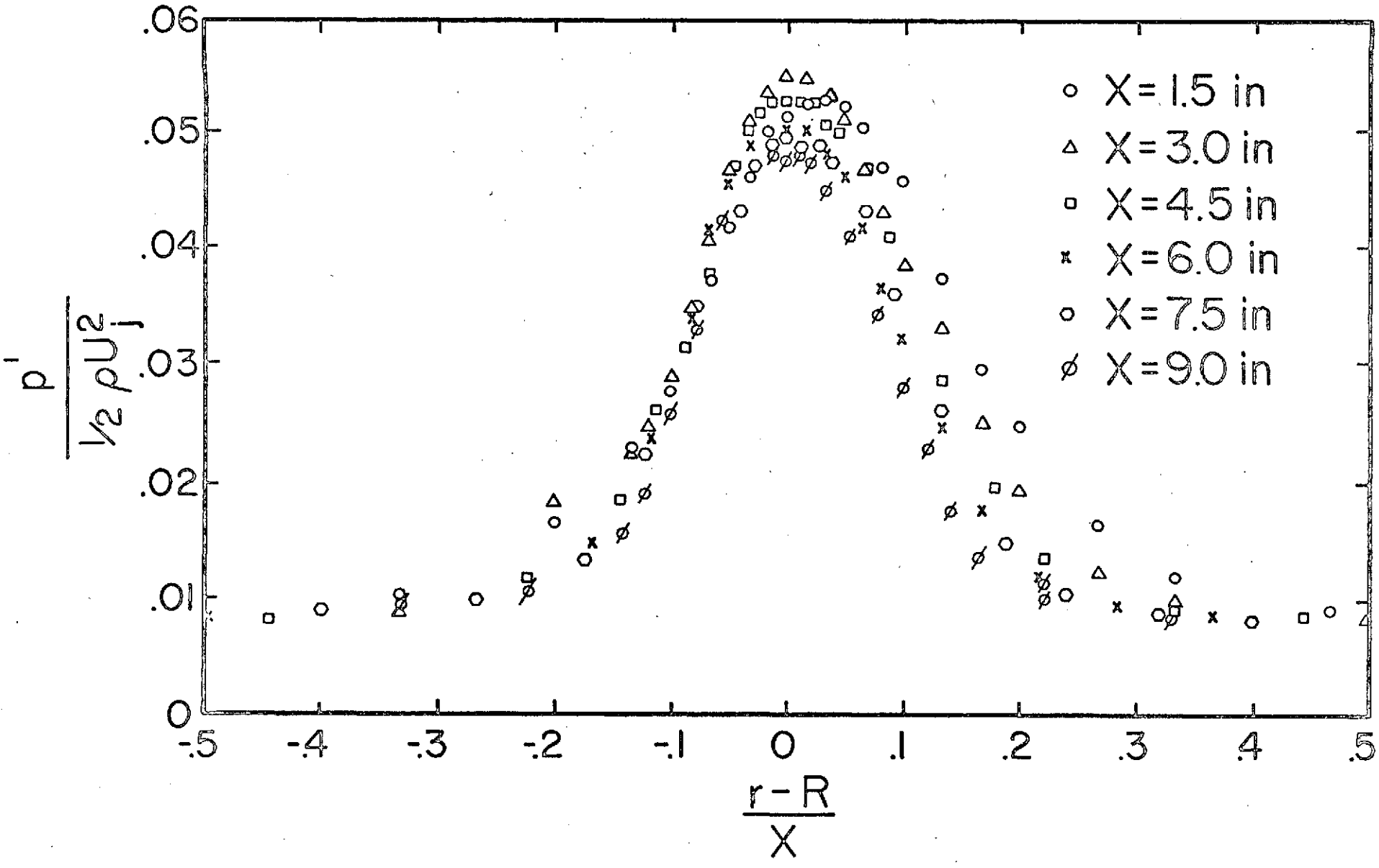

Fig. 13 RMS fluctuating static pressure profiles (NASA 6 in. dia. jet: $\overline{U}_j \approx$ fps, $\frac{1}{2} \rho \overline{U}_j^2 = 41.5$ in. water)

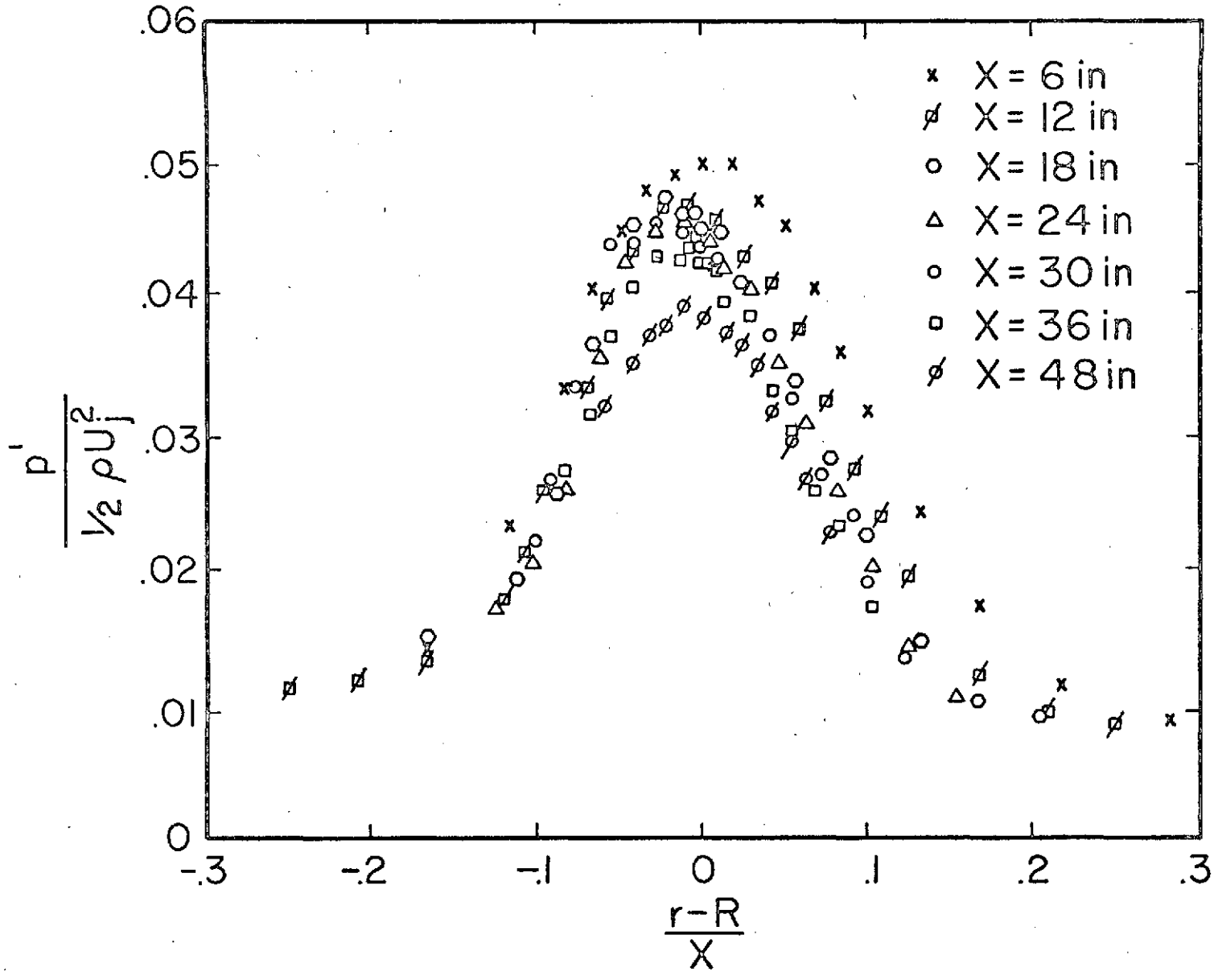

Fig. 14 RMS fluctuating static pressure profiles (NASA 6 in. dia. jet: $U_j \simeq 400$ fps, $\frac{1}{2} \rho U_j^2 = 41.5$ in. water)

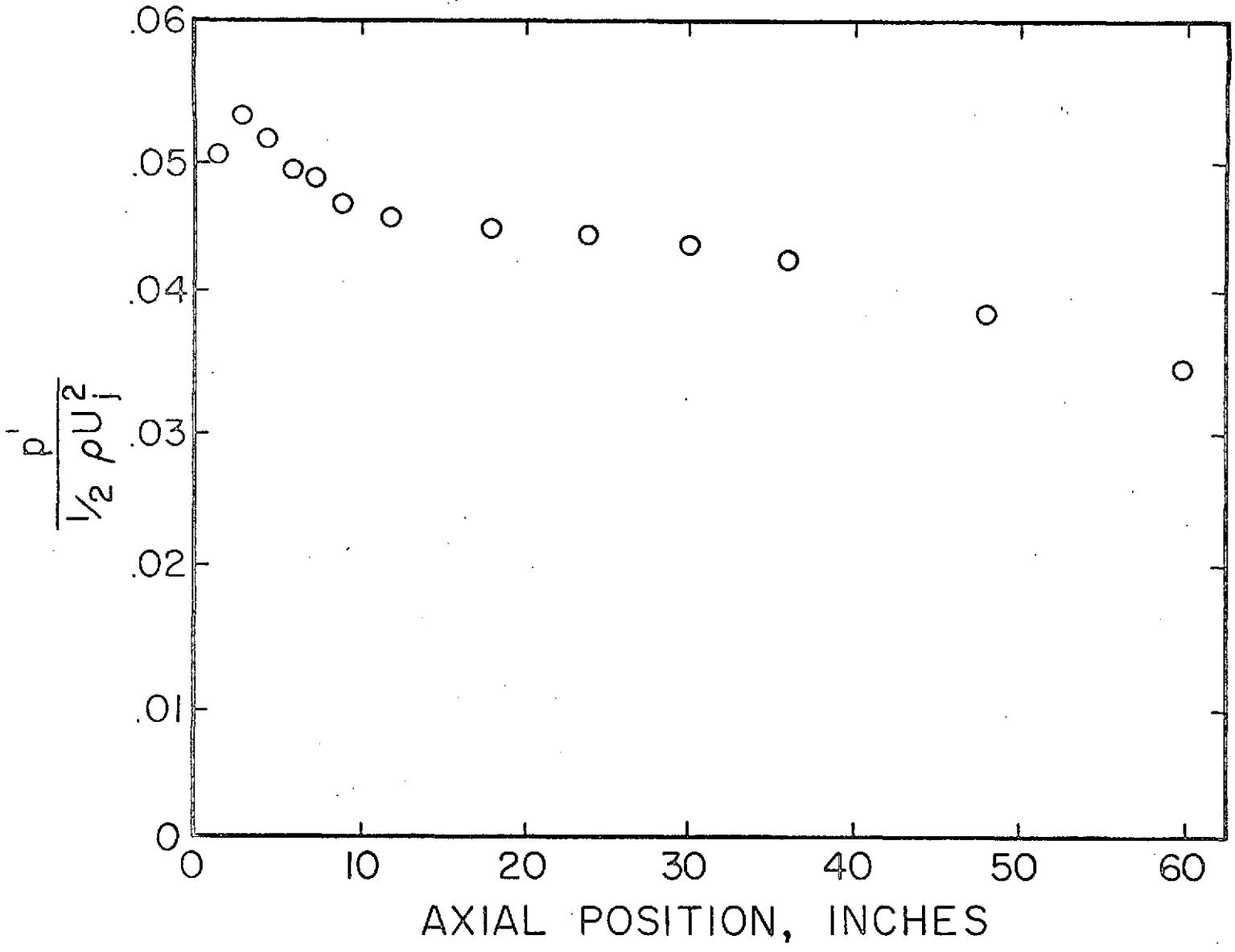

Fig. 15 Peak RMS fluctuating static pressure intensities (NASA 6 in. dia. jet: r near center of mixing, $U_j \simeq 400$ fps, $\frac{1}{2}\rho U_j^2 = 41.4$ in. water)

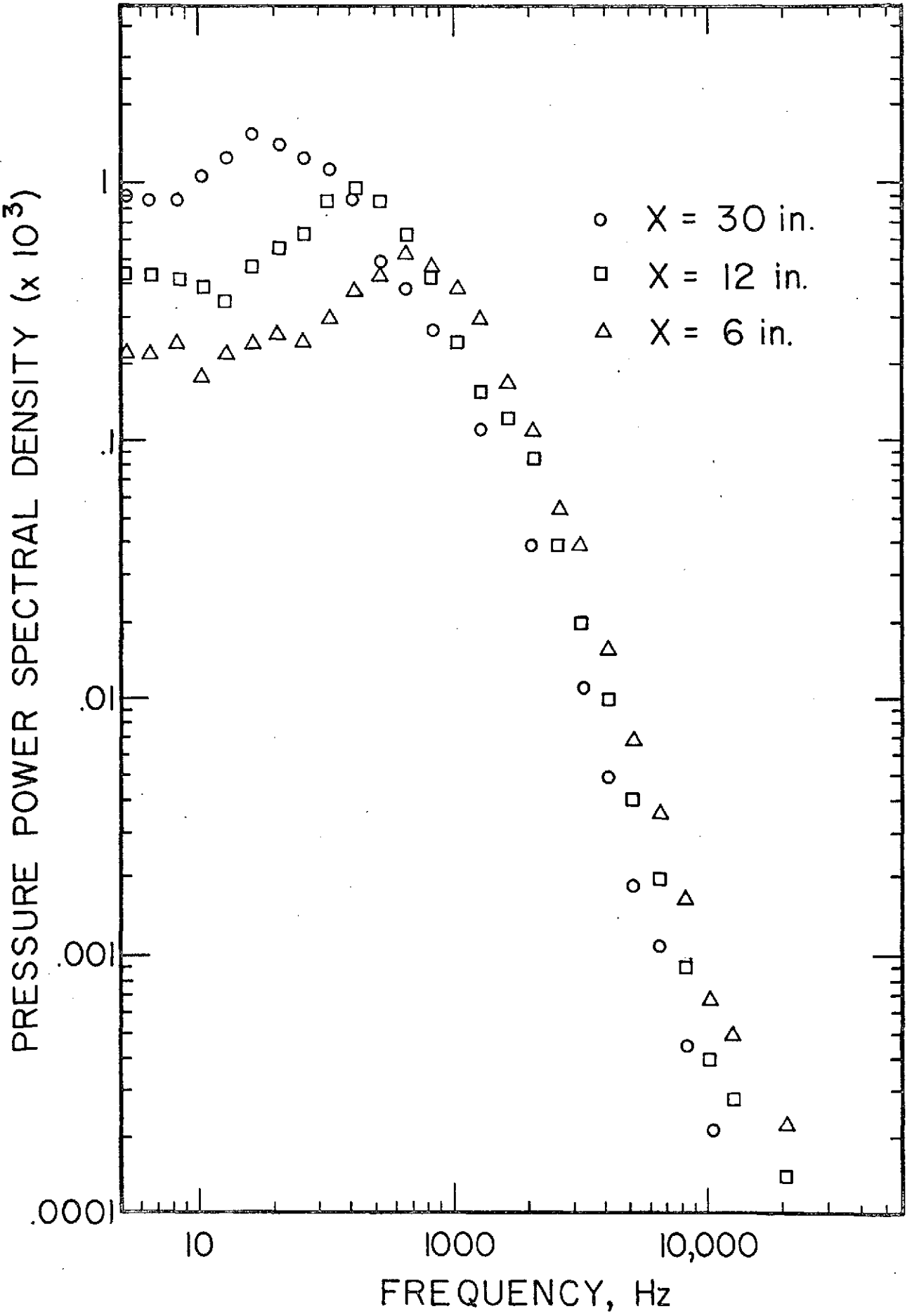

Fig. 16 Fluctuating static pressure spectra (NASA 6 in. dia. jet: r = 3.0 in., $U_j \simeq 400$ fps).

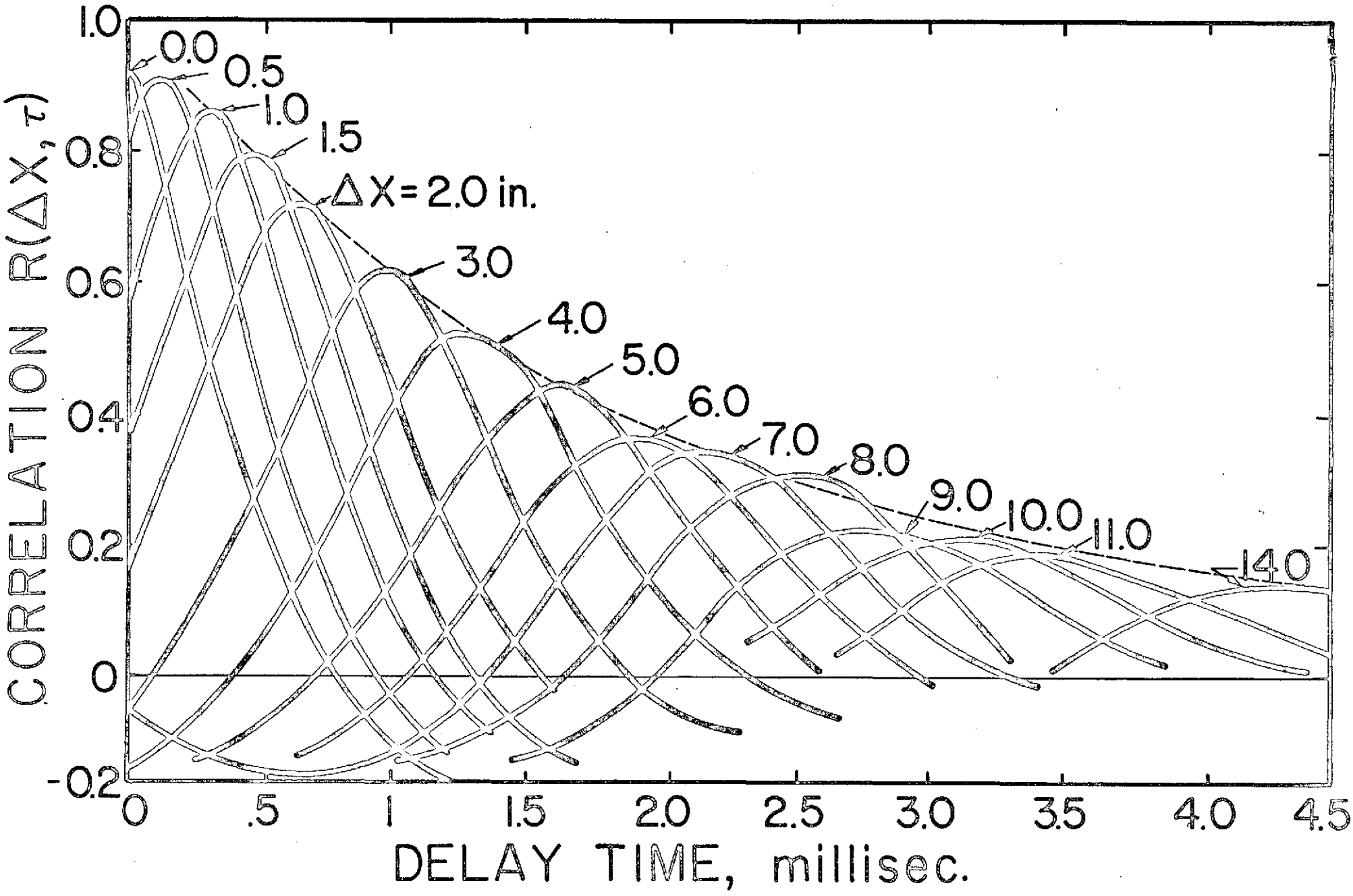

Fig. 17 Fluctuating static pressure axial space time correlations (NASA 6 in dia. jet: upstream probe at X = 24 in., both probes at r = 3.0 in. and $U_j \approx 400$ fps).

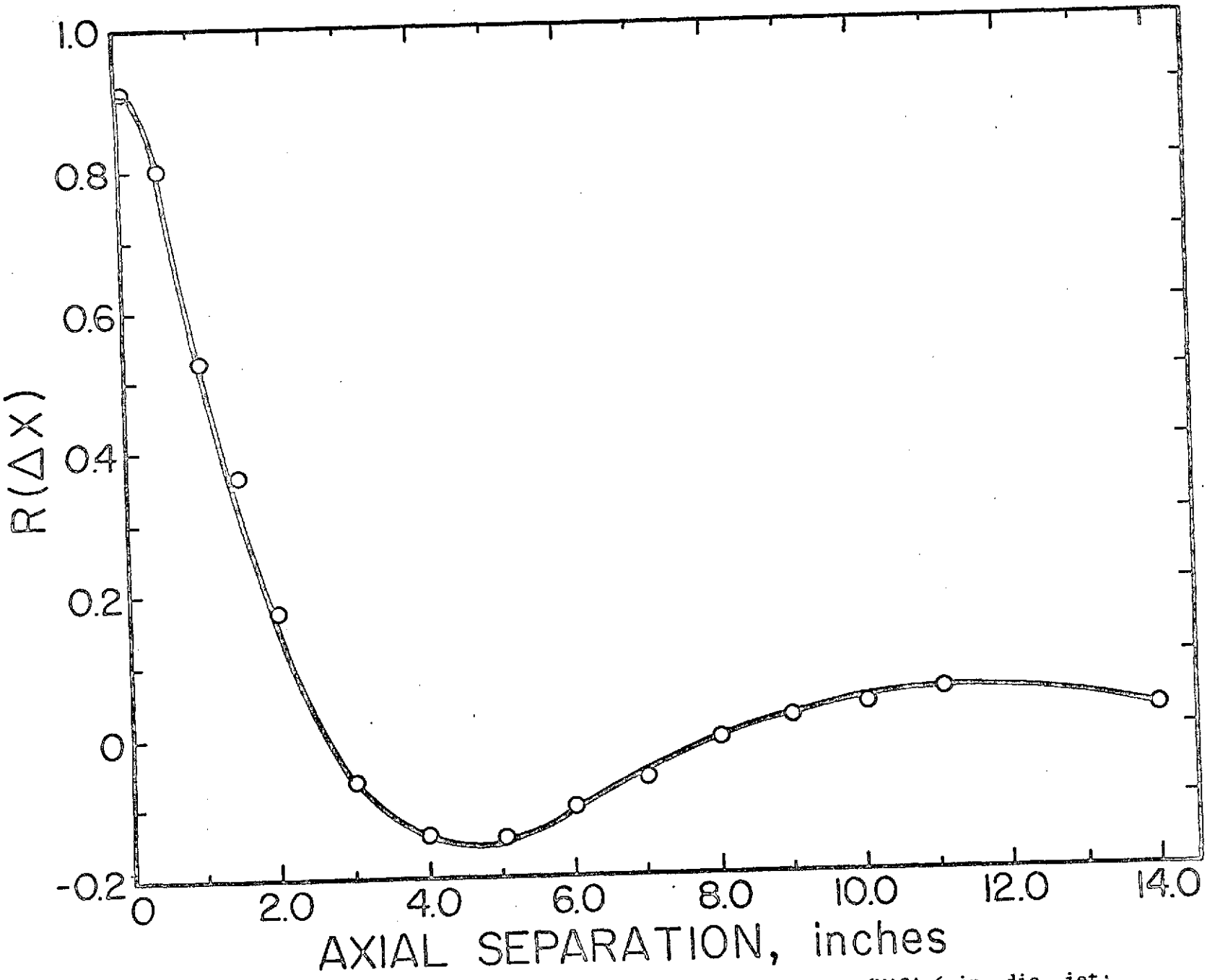

Fig. 18 Fluctuating static pressure axial space correlation (NASA 6 in. dia. jet: X = 24 in., r = 3.0 in., $U_j \approx 400$ fps)

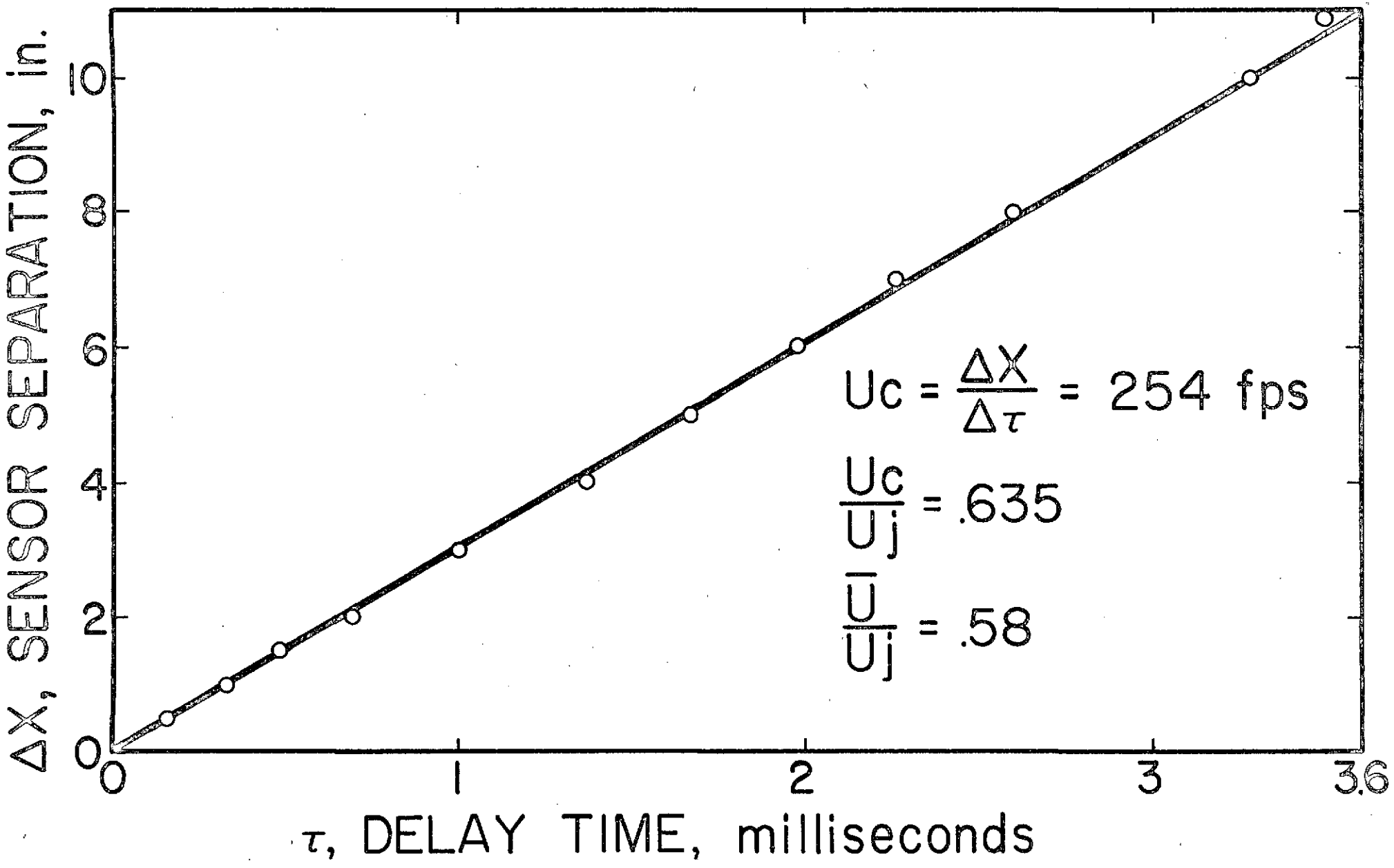

Fig. 19 Pressure correlation axial convection velocity (NASA 6 in. dia. jet: X = 24 in., r = 3.0 in.)